JOURNAL OF SPACECRAFT AND ROCKETS
Vol. 39, No. 2, March–April 2002

Modeling of the Interaction of a Side Jet with a Rarefied Atmosphere

S. F. Gimelshein*
George Washington University, Washington, D.C. 20052
and
A. A. Alexeenko† and D. A. Levin‡
Pennsylvania State University, University Park, Pennsylvania 16802

The interaction of a jet from a 3000-N-class thruster positioned on the side of a small rocket, with the rarefied atmosphere at 100 and 80 km, is studied numerically. The direct simulation Monte Carlo method was applied to model the three-dimensional jet-atmosphere interaction. Chemical reactions between freestream and plume species were included in the simulations. A two-stage numerical strategy was used, with sequential computations of an axisymmetric plume core flow and three-dimensional plume-freestream interaction. The impact of altitude, angle of attack, rocket velocity, and thrust on flowfields and surface mass fluxes is examined.

Introduction

SPACE vehicles often use divert and attitude reaction control systems (RCS) to perform maneuvers during flight. The forward and aft RCS engines provide the thrust for attitude (rotational) maneuvers (pitch, yaw, and roll) and for small velocity changes along the vehicle trajectory (translation maneuvers). The application of RCS is particularly important at high altitudes where the efficiency of the control surfaces decreases significantly as a result of the low density of the freestream. It is therefore needed to predict the effects of the interaction of RCS jets with the rarefied atmosphere accurately. The experimental study of jet-atmosphere interaction is hardly able to match similarity parameters of such an interaction,[1] making a detailed numerical simulation indispensable. The description of the interaction of RCS jets with the rarefied atmosphere is configuration specific.[2] That means that the available experimental data for the Space Shuttle Orbiter[3] and the sharp leading-edge jet-interaction measurements[4] are not applicable to other vehicle types.

Computations of RCS jet interactions in rarefied atmospheres were undertaken by various authors.[5–8] The modeling efforts were concentrated on different aerodynamic aspects of the RCS: freestream interaction and different vehicle types in a perfect gas environment. The direct simulation Monte Carlo (DSMC) method was used[1] to compute the three-dimensional jet interaction for a corner flow configuration; the results were compared with experimental data of surface-pressure distributions. A sharp leading-edge configuration[2,7] was also used where both the kinetic (DSMC) and continuum approaches were utilized to model in detail the interaction between a continuum jet and the rarefied atmosphere. The flow separation effects were studied[6] for a biconic atmospheric interceptor geometry and near-continuum atmosphere conditions of 65 km. The recent work[8] examines transient effects associated with jet interactions at 20 and 35 km for a generic interceptor missile configuration.

The previous results obtained by continuum and kinetic approaches showed the importance of an accurate and detailed modeling of the jet-atmosphere interaction to obtain a credible solution of space vehicle aerodynamics. Another important feature of the jet interaction not previously studied is the chemical reactions between the jet and atmospheric species that would affect the operation of onboard sensors. It is known[9] that for a range of rocket speeds and altitudes there exists the potential for the exhaust thruster species to radiate and interfere with optical sensors. The accurate modeling and simulation of the jet-atmosphere interaction is a prerequisite for computing the spatial mapping of the contaminant radiation. This endeavor is complicated by many considerations: 1) the flow geometry is three dimensional, 2) the density in the flow and species concentrations can vary by many orders of magnitude, and 3) chemical reactions occur between the thruster plume gases and the ambient atmosphere.

The main goal of this work is the multiparametric study of the three-dimensional interaction between the forward RCS jet of a small rocket and an ambient rarefied atmosphere at 80 and 100 km, with special attention paid to the examination of possible contamination of the onboard radiance sensor located on the cylindrical part half a meter downstream from the nozzle. An important issue of this work is the numerical accuracy of the modeling of flowfields, surface mass flux, and chemical reactions between the plume and atmospheric species. The impact of rocket velocity, thrust level, angle of attack, and flight altitude on the distributed mass flux is studied. The DSMC method is used in this work as the main predictive tool. This work represents a new application of the DSMC method to the study of the jet-atmosphere interaction with a chemical reaction model. The solution of Navier–Stokes equations for the jet in the vicinity of the nozzle exit is also presented for the comparison with the DSMC results.

In the following section the statement of the problem is presented along with the definition of geometric setup and flow conditions. The numerical approach used in the computations is discussed, and the main computational steps are given for the full three-dimensional modeling of a rocket side jet interacting with the atmosphere at high flight altitudes. Comparison of plume modeling results obtained using kinetic and continuum techniques is shown. Finally, results related to the impact of different jet and freestream parameters are also presented.

Flow Conditions

A schematic of the flow geometry utilized to study the interaction of atmosphere and the RCS jet is given in Fig. 1. A small rocket is modeled as a blunted cone cylinder, and the thruster is positioned on the cylinder, right after the cone-cylinder junction. An important issue of this work is the examination of possible contamination of the onboard radiance sensor located on the cylindrical part half a meter downstream from the nozzle. The angle of attack is zero on the schematic, but other values of the angle of attack are also considered.

Received 16 March 2001; revision received 31 August 2001; accepted for publication 5 September 2001. Copyright © 2001 by the American Institute of Aeronautics and Astronautics, Inc. All rights reserved. Copies of this paper may be made for personal or internal use, on condition that the copier pay the $10.00 per-copy fee to the Copyright Clearance Center, Inc., 222 Rosewood Drive, Danvers, MA 01923; include the code 0022-4650/02 $10.00 in correspondence with the CCC.

*Senior Research Scientist, Department of Chemistry; gimel@gwu.edu.
†Graduate Student, Department of Aerospace Engineering; alexeenko@psu.edu. Student Member AIAA.
‡Associate Professor, Department of Aerospace Engineering; dalevin@psu.edu. Senior Member AIAA.

Table 1 Freestream parameters

Parameter	Case 1	Case 2
Altitude, km	80	100
Temperature, K	181	186
Number density, molecules/m^3	4.18×10^{20}	1.26×10^{19}
O_2 composition, %	21	15.9
N_2 composition, %	79	79.4
O composition, %	0	4.7

Table 2 Nozzle-exit conditions

Condition	Value
Concentration	
H_2O	25%
CO_2	5%
CO	23%
HCl	14%
N_2	14%
H_2	19%
Velocity	2540 m/s
Temperature	650 K
Number density	7.29×10^{23} molecule/m^3
Nozzle-exit area	176.7 cm^2
Wall temperature	300 K

Table 3 Freestream-plume species reactions

Reagent	Product	A, m^{3}s	B	E_r, J
$N_2 + H_2O$	$N_2 + OH + H$	5.8×10^{15}	0.0	7.3×10^{19}
$O_2 + H_2O$	$O_2 + OH + H$	1.13×10^{7}	−1.31	8.1×10^{19}
$O + H_2O$	2OH	3.8×10^{21}	1.3	1.2×10^{19}
$N_2 + OH$	$OH(A) + N_2$	9.4×10^{17}	−0.37	6.4×10^{19}
$O_2 + OH$	$OH(A) + O_2$	9.4×10^{17}	−0.37	6.4×10^{19}
O + HCl	OH + Cl	5.6×10^{27}	2.87	0.2×10^{19}
OH + Cl	O + HCl	3.1×10^{27}	2.91	0.7×10^{20}

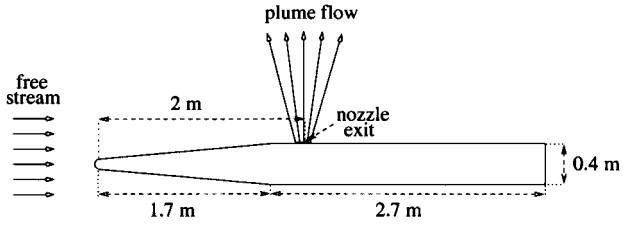

Fig. 1 Schematic of the flow.

The flow at two flight altitudes is modeled: 80 and 100 km. Table 1 gives the freestream parameters used for these altitudes. Three different values of the free stream velocity U_∞ were assumed: $U_\infty = 2$, 3, and 4 km/s.

The plume nozzle-exit conditions corresponding to a thrust of $F = 3250$ N the number density of 7.29×10^{23} molecule/m^3) are given in Table 2. The thrust values of $F = 6500$ N were also used in several calculations, implying a number density of 1.458×10^{24} molecule/m^3, and all other parameters remain the same. A constant distribution over the nozzle exit for the thruster exhaust species was assumed.

The gas composition at the nozzle exit was assumed to be typical for small divert thrusters[9] with a solid nonaluminum propellant, and only the major species were used in the approximation. Chemical reactions were included both between the freestream species and the freestream-plume species. The freestream chemical reaction set consists of 15 dissociation and 4 exchange reactions between the air species. The reaction data used for these reactions can be found elsewhere.[10] It will be shown that the freestream reactions impact the flow only for those cases with the higher freestream velocity. The reduced set of chemical reactions used to model the interaction between the plume and atmospheric species and corresponding Arrhenius reaction rate constants $k_r = AT^B \exp(-E_r/kT)$ are listed in Table 3.

There are three types of reactions included in the table. The first three reactions represent the dissociation of water by impact with ambient species to form OH and H. The fourth and fifth reactions represent the collisional excitation of ground state OH to form $OH(A)$. Finally, the last two reactions represent mechanisms for the formation of free chlorine radicals, an important precursor in atmospheric models of ozone depletion.

Computational Technique

The numerical challenge of the problem under consideration is associated with the flow three-dimensionality and a large variation in number density. The flow regime changes from continuum at the nozzle throat (number density on the order of 10^{24} and the nozzle diameter-based Knudsen number on the order of 10^{-5}) to transitional in the freestream (number density of 10^{19} at 100 km). Thus, the continuum approaches cannot be applied to simulate most of the flow, and a kinetic approach has to be used. The most widely used and powerful kinetic technique is the DSMC method,[11] a method that has been shown to be efficient for various gas dynamic problems in the free-molecular, transitional, and near-continuum flow regimes. A multitask DSMC-based computational tool, SMILE,[12] is used in this work.

The continuum method is also applied in this work for the plume near field to validate the DSMC solution in the high density region. The solution of the Navier–Stokes equations with a finite volume spatial discretization on a structured grid is obtained with the General Aerodynamic Simulation Program (GASP).[13] The six-species gas mixture is computed with the Sutherland model used to approximate the temperature dependence of the gas viscosity. Viscous derivative terms in the momentum and energy conservation equations are computed with second-order accuracy on the interior and gas-solid interface cells. The third-order upwind-biased scheme is applied for spatial reconstruction of volume properties on the cell boundaries. To obtain a steady-state solution, two-factor approximate factorization is used for time stepping.

Numerical Strategy

The DSMC method becomes prohibitively expensive when it is applied to modeling three-dimensional flows at very low Knudsen numbers. Because the gas density for the flow of interest is very high at the thruster exit, a full three-dimensional modeling of the jet-atmosphere interaction problem would require a large number of simulated molecules to be used. To obtain an accurate flow solution requires a large number of particles to reduce the statistical dependence between simulated particles.[14]

The numerical strategy implies a splitting of the flow into two regions: the plume near field where the flow is essentially axisymmetric and the region of the three-dimensional freestream plume. In the modeling of the plume near field, computational requirements can become prohibitive and therefore reduce the fidelity and accuracy of the solution. Thus two different approaches, kinetic and continuum, were used to obtained a credible solution for the plume near field. The plume is modeled as a six-species (see preceding section) nonreacting gas mixture expanded into a vacuum.

For the continuum approach, the solution of the Navier–Stokes equations for the plume near field was obtained using GASP.[13] The flow was modeled with different axisymmetric grids to obtain a grid-independent result. The continuum approach is certainly valid for this regime, except for the relatively low-density regions of side flow and plume far field.

Because the final goal is to simulate the jet-atmosphere interaction, an accurate prediction of side portion of the plume flow is important. The axisymmetric capability of SMILE was therefore used to calculate plume near field concurrently with the continuum approach. Calculations were performed with various cell sizes and numbers of simulated molecules in order to obtain a solution independent of these numerical parameters.

The main step of the calculation is the modeling of the jet-atmosphere interaction. The three-dimensional SMILE tool is used to compute the interaction of the freestream and plume species. The gas is considered a 13-species reacting mixture. A starting surface

obtained with the axisymmetric DSMC code is used to simulate the plume inflow.

Plume Near-Field Simulation

The continuum and kinetic approaches were used to model the plume near field at $F = 3250$ N, and the most important parameters of the approaches were varied to obtain a reliable solution. Three different grids were used to model the plume using GASP: 100×50, 300×150, and 600×200 cells (The first dimension is along the plume axis direction.). Figure 2 shows a comparison of the plume number density along the plume axis for all three grids. It can be seen that the second and third grids provide the same distribution. The third grid therefore represents a grid-independent result.

The DSMC calculation of the plume near field was performed for three different sets of numerical parameters. For each set the following values were used for the total number of molecules and cells, respectively: 1) 30,000 and 7000; 2) 600,000 and 300,000; 3) 1,100,000 and 500,000. Figure 3 shows the calculated number densities for the three different parameter sets. The sensitivity of the solution to the number of simulated molecules and cell size is not as significant as was observed for the continuum calculation grid comparison. The third DSMC parameter set is assumed to provide a result that is independent of both the grid size and the number of particles.

Comparison of the continuum and DSMC plume near-field solutions showed that the general features of the plume—pressure contours and density (e.g., Figs. 2 and 3) and temperature distributions along the plume axis—were in good agreement. However, comparison of the properties in the plume side flow (large angles off the plume axis) shows potentially serious disagreement between the Navier–Stokes and DSMC solutions. Figure 4 shows a comparison of the angular dependence of the number density for a distance of 0.75 m from the nozzle exit center for the two numerical methods. It can be seen that in the side portion of the plume, which is more rarefied than its core, there is a significant disagreement between the two approaches. It is likely that the GASP Navier–Stokes solution fails to predict accurately the regions of high flow rarefaction.

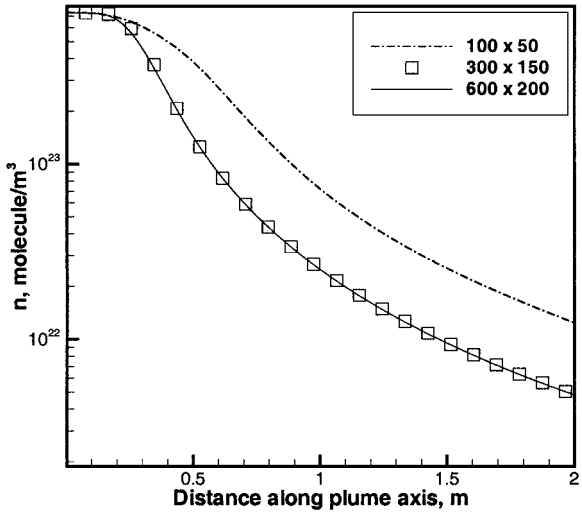

Fig. 2 Continuum number density distribution along the plume axes for different grids.

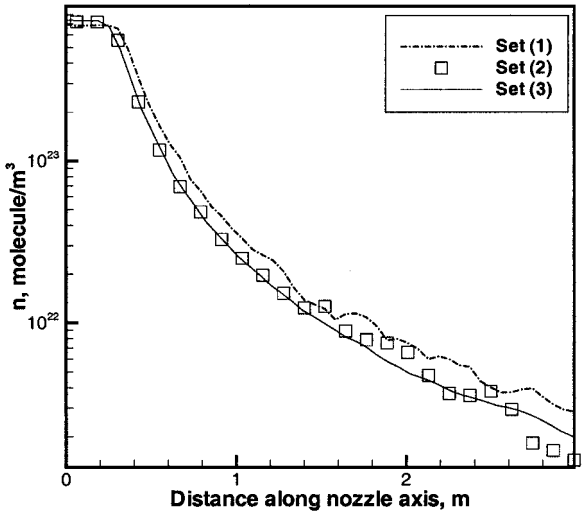

Fig. 3 DSMC number density distribution along the plume axis for the three parameter sets.

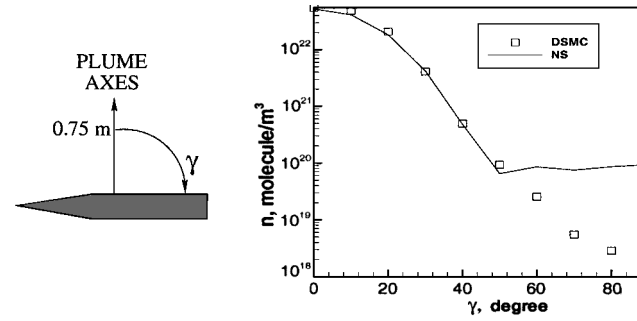

Fig. 4 Comparison of the angular dependence of the number density at 0.75 m for DSMC and NS methods.

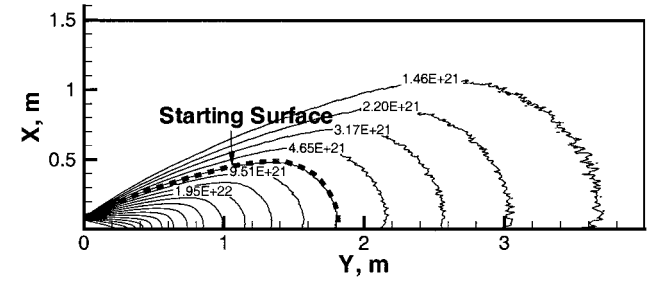

Fig. 5 Starting surface shown along with the axisymmetric plume number density contours (molecule/m^3).

Starting Surface for Three-Dimensional Simulations

The computational requirements for treating the entire three-dimensional problem with the DSMC method for the conditions considered here are considerable. Therefore to facilitate the calculation, the plume solution is assumed to be axisymmetric for some region close to the nozzle exit. Clearly as the plume gas moves away from the thruster and interacts with the freestream, this assumption is no longer valid. Hence there has to be a hand-over from the axisymmetric plume solution to the full three-dimensional one. The hand-over occurs in the region where the plume density is too high for the plume to be affected by the freestream, thus providing a starting surface for full three-dimensional simulations. The density isolines of $\sim 7 \times 10^{21}$ and $\sim 1.3 \times 10^{22}$ molecule/m^3 were taken for the starting surfaces of the 3250- and 6500-N thrusters, respectively. The parameters at the surface, such as flow direction, velocity, and temperature, were taken from the axisymmetric DSMC simulations. The difference between the translational temperatures in X and Y directions was found to be insignificant at the starting surface, and a Maxwellian distribution function was therefore used for molecules entering the domain from the starting surface. Note that the Bird's breakdown parameter[15] for a 3250-N thruster changes from 0.04 at the nozzle throat to 0.002 farther downstream, which also substantiates the use of the Maxwellian distribution function. Figure 5 shows the number density contours for the plume near fields for a 3250-N thruster [set (3) of the DSMC numerical parameters] and the starting surface used in this case.

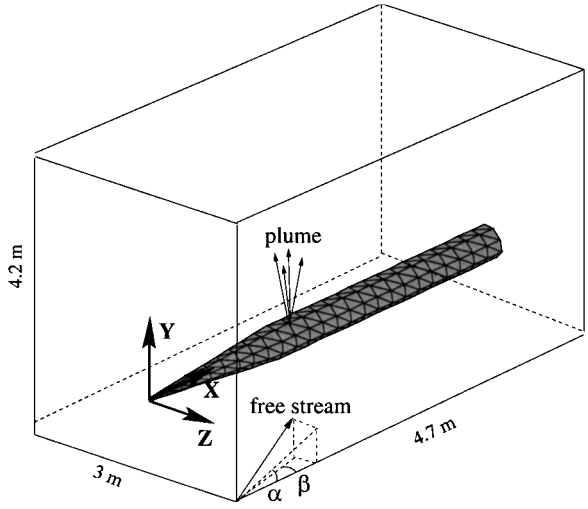

Fig. 6 Schematic of the three-dimensional computational domain and axis notations.

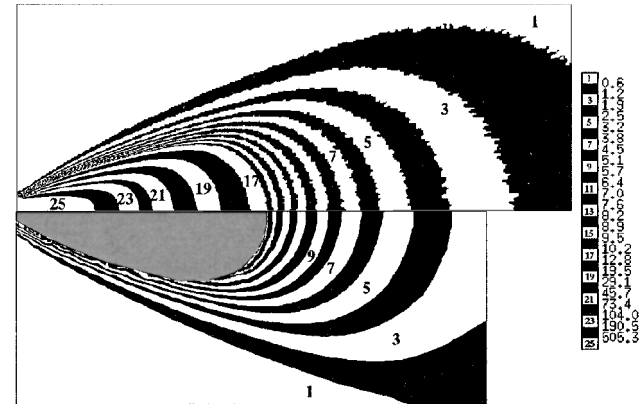

Fig. 7 Comparison of two-dimensional (top) and three-dimensional (bottom) pressure fields (Pa). The area shown is 4 × 1.5 m for two-dimensional and 3.5 × 1.5 m for three-dimensional fields.

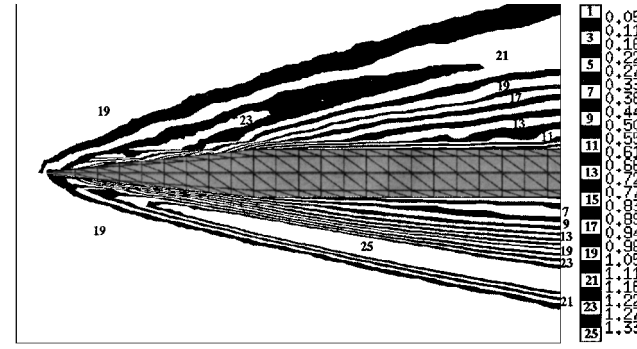

Fig. 8 Normalized number density contours about a small rocket at 100 km (top half) and 80 km (bottom half). The area shown is 4.7 × 1.5 m for each altitude.

DSMC Models and Three-Dimensional Numerical Parameters

The models and numerical parameters utilized in the three-dimensional DSMC computations are as follows. The variable hard sphere model[16] was used for intermolecular collisions. The Larsen–Borgnakke model[17] with temperature-dependent rotational and vibrational relaxation numbers was assumed for the energy transfer between the translational and internal molecular modes. The total collision energy[16] model was applied to model gas-phase chemical reactions. A weighting scheme[18] applicable for chemical reactions was used to enhance the statistical representation of freestream species. The diffuse model with total energy and momentum accommodation was taken for the gas-surface interaction with the rocket wall temperature of 300 K.

A schematic of the computational domain is shown in Fig. 6, where the direction of the axes, the plume, and the freestream is also shown. The beginning of the coordinate system is placed at the nose tip. The total number of cells is about 3 million (from 2.5 to 3.6 million depending on the freestream and plume parameters), and the number of simulated molecules was in the range of 4–6 million. These numerical parameters were chosen to eliminate the grid dependence of the results, reduce the influence of statistical dependence between the simulated particles, and provide an adequate spatial resolution of the boundary layer along the rocket. One calculation for a 3250-N thruster was performed with 5.2 million cells and about 15 million particles, and the results were found to be the same as for the baseline case of 2.5 million cells and 4.5 million molecules. A typical three-dimensional computation took about two days on 24 processors of an IBM SP/RS6000 POWER3 computer.

Results and Discussion

Plume Structure with No Freestream

Each of the three-dimensional calculations starts with modeling the rocket thruster plume exhaust into a vacuum. The goal of these first calculations is twofold. First, the comparison of two- (as described in the preceding sections) and three-dimensional results permits the verification of the choice of numerical parameters for the three-dimensional modeling. Second, the three-dimensional computations of flow into a vacuum enable one to compare the mass flux from a single jet to the rocket surface with no impact of the freestream to that of the atmosphere-jet interaction case. The numerical parameters verification is discussed in this section, and the comparison of distributed surface mass fluxes is presented in the following sections.

A comparison of the pressure contours obtained using the two- and three-dimensional codes is presented in Fig. 7 for the 3250-N-thruster case. The three-dimensional results are shown in the *YZ* plane. Only a portion of the computational domain is shown for the three-dimensional case for the sake of clarity. Here and in other figures the gray area shows the portion of the domain bounded by the starting surface. The figure illustrates an excellent agreement between the two- and three-dimensional pressure contour results, both in the outer edges of the plume and downstream along the plume axis. Similar agreement is observed for other macroparameters. The agreement between the results shows that the numerical parameters chosen allow one to accurately capture the plume structure, which is the portion of the flow that has the most challenging computational requirements. Good agreement between the two- and three-dimensional plume structure was also obtained for the 6500-N thruster.

Flow About a Small Rocket at Different Altitudes Without the Side Jet

To better understand the impact of the side jet on the mass flux to the surface and flow parameters, the flowfield was calculated at different altitudes with and without the jet. The flowfields without the jet are presented in this section. The freestream gas is air, the angle of attack is 0 deg, and the freestream velocity is 2 km/s. Although air chemical reactions were included in the simulations, their impact is negligibly small at this velocity. This is because the shock wave is weak and the translational temperature in the shock front does not exceed 1000 K.

Total number density contours normalized by the freestream value are shown in Fig. 8 (upper half) for an altitude of 100 km. The density in the shock layer reaches only 1.25 of its freestream value and decreases to 0.5 closer to the body. The impact of the bow shock on the jet is expected therefore to be small. Generally, the shock wave is wide and merges with the boundary layer at these highly rarefied conditions. (The Knudsen number based on the cylinder diameter is 0.25.) The shock wave is predictably more pronounced at a lower altitude. An illustration of the flow structure at 80 km is shown in the bottom half of Fig. 8. The number density reaches its maximum of about 1.5 and drops in the boundary layer to about 0.3 of its freestream value.

The distributed total mass flux along the body for the two altitudes is presented in Fig. 9. Hereafter, the X axis is the distance in meters from the nose tip to the rear part in XY plane ($Z = 0$). There is a

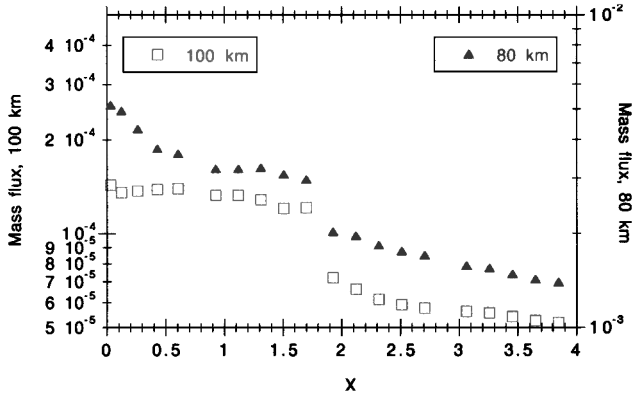

Fig. 9 Total mass flux (kg/m^{2}s) along a small rocket at 80 and 100 km.

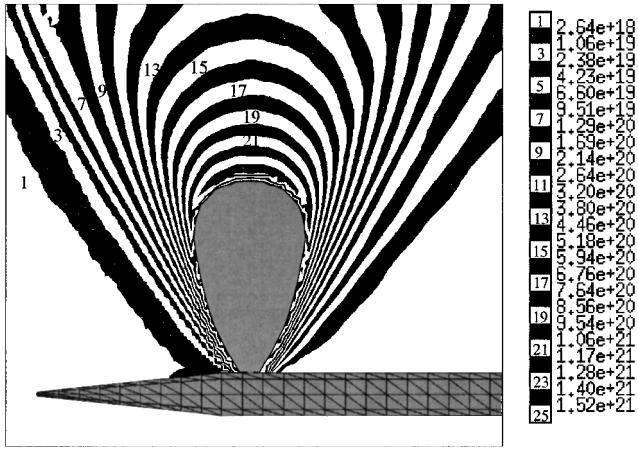

Fig. 10 Plume H_2O number density (kg/m^3). *XY* plane ($Z = 0$). The area shown is 4.7 × 4.2 m.

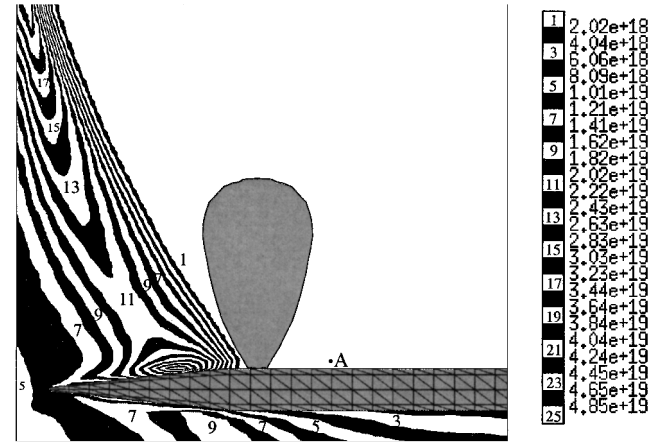

Fig. 11 Freestream N_2 number density (kg/m^3). *XY* plane ($Z = 0$). The area shown is 4.7 × 4.2 m.

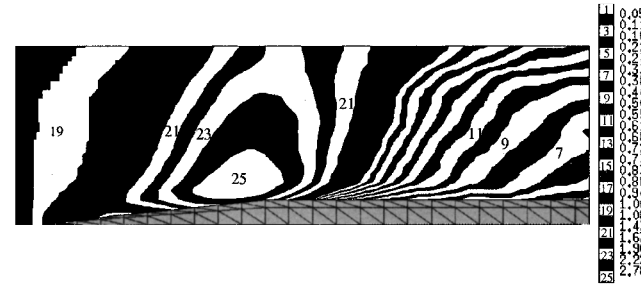

Fig. 12 Total number density normalized by the freestream value. *XZ* plane ($Y = 0$). The area shown is 4.7 × 1.5 m.

visible increase in the mass flux in the vicinity of the nose for 80 km. The increase is caused by the gas mean free path comparable to the nose radius in this case, which causes the formation of the detached shock wave with a significantly higher density in the vicinity of the nose. A decrease of approximately 50% in the mass flux is observed on the cylinder junction as compared to the cone portion of the rocket for both altitudes. The difference between the mass-flux values on the cylindrical part for the two altitudes is proportional to the difference in the freestream number densities.

Modeling of the Freestream-Plume Interaction

Consider now the modeling of the jet-atmosphere interaction. The results for a 3250-N thruster and a freestream velocity of 2 km/s with zero angle of attack at 100 km are presented in this section.

The number density contours of the main plume species, H_2O, are presented in Fig. 10. The portion of the flow in the *XY* plane that is formed by the rocket symmetry axis and the plume axis is shown. Here and in the following the spatial scale corresponds to that shown in Fig. 6. Again, the black line around the gray area shows the starting surface taken from the axisymmetric DSMC computations. The principal conclusion here is that the influence of the freestream on the plume is small for these freestream conditions. There is only a small difference between the left portion of the plume, which is affected by the plume, and the right, lee side, portion. This difference is only observed for the regions where the plume density is smaller or slightly larger than that of the freestream. Also, there is no noticeable effect of the rocket bow shock on the H_2O number density field.

The number density of the main freestream species, N_2, is shown in Fig. 11. There is a significant nitrogen number density in the plume, but the number density of those molecules is not shown in this figure. The freestream and plume nitrogen molecules were treated as two different species. Figure 11 clearly shows that a shock wave is formed in front of the plume as a result of the atmosphere-jet interaction. The density in the shock increases to about 4.5 times compared to the freestream value because of the impact of the internal degrees-of-freedom excitation. (The maximum increase is four times for a monoatomic gas.) The maximum freestream N_2 number density appears in the vicinity of the wall as a result of the bow shock–rocket body–plume interaction. Although there is no penetration of the freestream molecules in the plume core flow, there is some amount of the freestream nitrogen above the cylinder right behind the plume (point A with the number density of $2. \times 10^{17}$ molecule/m^3). This amount is expected to be a significant contributor to the surface mass flux in the area where a radiance sensor might be located.

The flowfield results show that the jet flow influences not only the flow on the side of the rocket where it is directed but also the flow in the entire area of the rocket. An example is given in Fig. 12, where the gas total number density normalized by the freestream value is shown in the *XZ* plane. The *XZ* plane is the plane that passes through the rocket axis and is perpendicular to the plume direction. Only half of the computational domain is shown because the flow is symmetric with respect to the plume axis in the *XY* plane. The result is significantly different from what was obtained with no plume (compare Figs. 8 and 12).

The total mass flux along the rocket surface in the *XY* plane (as in Figs. 10 and 11) is shown in Fig. 13. Here and in the following the mass flux is calculated on the upper side of the body (positive *Y* values; Fig. 6). The mass flux has a maximum on the conical part of the rocket, corresponding to the maximum in the freestream gas number density in this region. Then it decreases two orders of magnitude along the cylindrical part. The mass flux for two species, freestream N_2 and plume H_2, is also shown in this figure. Nitrogen is presented as the main freestream species, with the freestream oxygen showing the same trend with the difference in magnitude proportional to the difference in the freestream concentrations. Hydrogen is shown here because it is the lightest species of the plume most affected by the freestream molecules and has therefore the biggest contribution to surface mass flux among all plume species. The mass flux from other plume species is several orders of magnitude less than that from hydrogen. The impact of the plume species on the mass

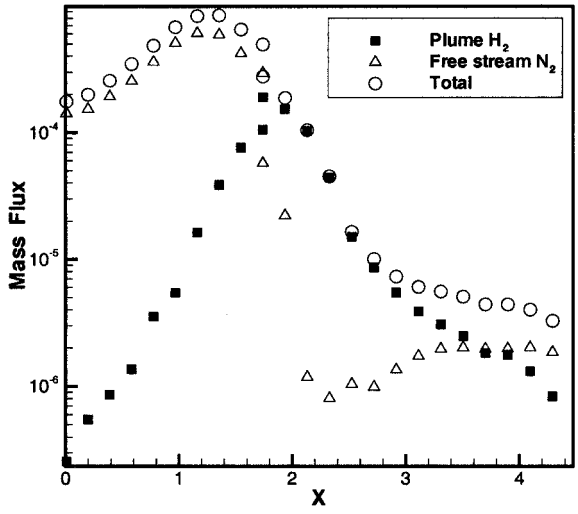

Fig. 13 Total and different species mass flux (kg/m^{2}s) along a rocket.

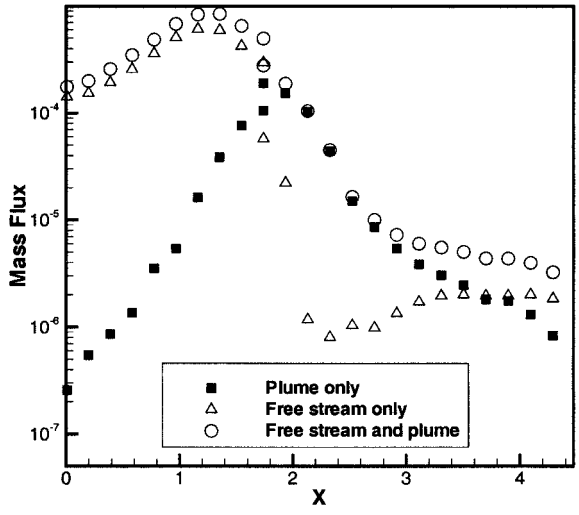

Fig. 14 Comparison of the total mass flux (kg/m^{2}s) with and without the freestream and plume.

flux on the surface is negligible for the conical portion of the body but significantly increases on the cylindrical part. The contribution of plume hydrogen at 0.5 m downstream from the nozzle, where a sensor might be located, is almost 100%. Farther downstream, the mass fluxes of plume H_2 and freestream N_2 are comparable.

Figure 14 gives more details on the influence of the jet-atmosphere interaction on the mass flux. Three different cases are presented: 1) the jet only with no freestream, 2) the freestream without the jet, and 3) the full jet-freestream case. The mass flux for 2) is larger than 1) along the surface, except for a small area close to the thruster. On the conical part of the body, the mass flux is obviously largest for 3). It becomes smaller than 2) downstream from the nozzle because of the shadowing effect of the plume.

Impact of the Freestream Velocity on the Flow Structure

Three different values of the freestream velocity were used in the computations, 2, 3, and 4 km/s, enabling one to analyze the effect of rocket velocity on the jet-atmosphere interaction. The results presented in this section were obtained for a 3250-N-thruster firing at an altitude of 100 km with zero angle of attack. Generally, the effect of the jet is expected to be larger at higher velocities because of a stronger shock wave produced by the jet interaction. Quantitative effects are evaluated next.

Comparison of Figs. 10 and 15 and Fig. 16 shows the impact of the freestream velocity on the plume structure. The H_2O number density contours are given in these figures, showing a visible difference between wind and lee sides of the plume for 4 km/s. The freestream gas pushes the plume molecules closer to the jet axis, and there

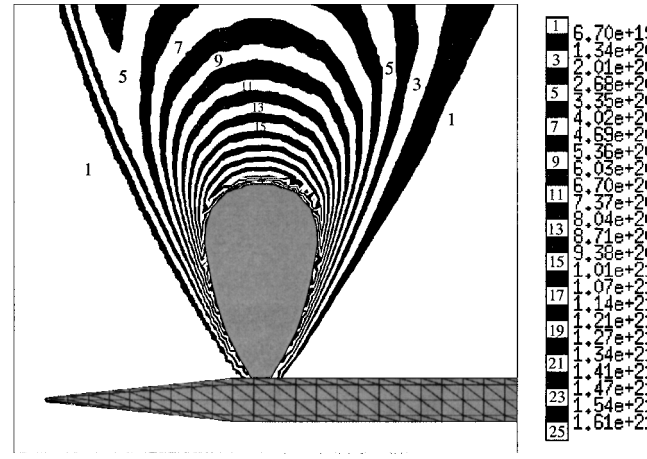

Fig. 15 Plume H_2O number density (kg/m^3) in XY plane ($Z = 0$) for U_∞ = 4 km/s. The area shown is 4.7 × 4.2 m.

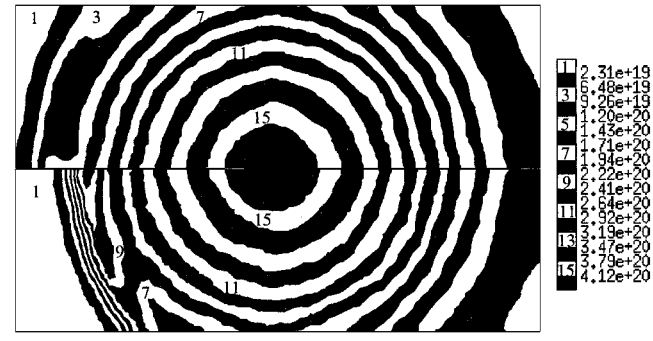

Fig. 16 Plume H_2O number density (kg/m^3) in XZ plane ($Y = 5.7$ m) for U_∞ = 2 km/s (top) and 4 km/s (bottom). The area shown is 4.7 × 1.5 m.

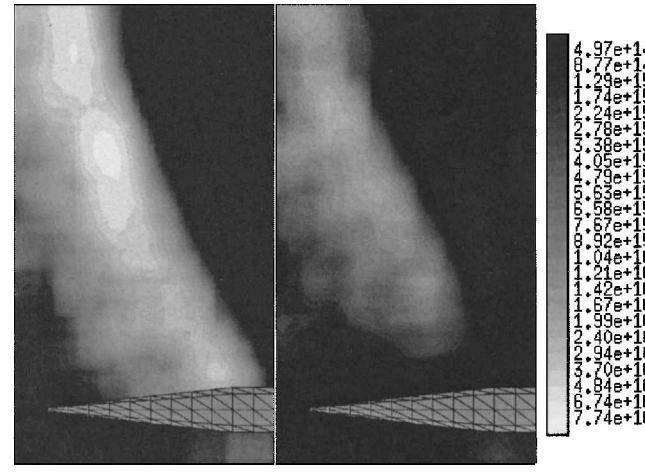

Fig. 17 Cl number density (kg/m^3) formed as a result of chemical reactions in XY plane ($Z = 0$) for U_∞ = 4 (left) and 3 km/s (right). The area shown is 4.7 × 4.2 m.

is a small local maximum of the H_2O number density seen in the windward portion of the plume.

Let us consider now the influence of the freestream velocity on chemical reactions between the freestream and plume species. The atomic chlorine number density fields are presented in Fig. 17 for 3 and 4 km/s. Atomic chlorine is produced by the reaction $O + HCl \rightarrow OH + Cl$, where O and HCl are freestream and plume species, respectively. Reactions between the plume and the freestream are rare event, and although the weighting scheme used reduces statistical scatter[18] the reaction product flowfields are still not as smooth as would be observed for a major species. However, it can be seen that atomic chlorine is produced in the the narrow region, where the freestream interacts with the plume and slightly penetrates

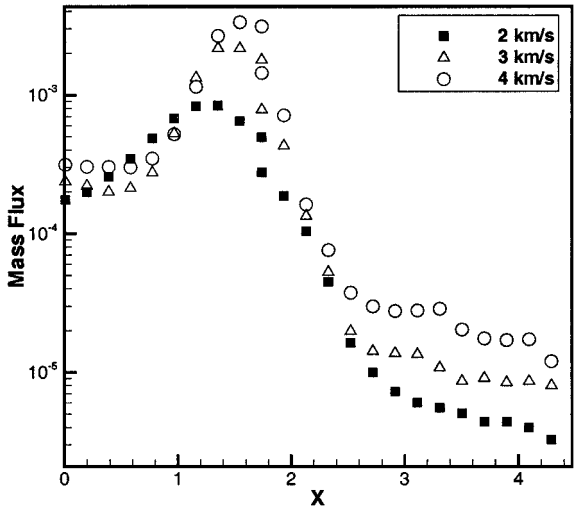

Fig. 18 Total mass flux (kg/m^{2}s) along a rocket for different freestream velocities.

upstream as a result of the low collision frequency at 100 km. Predictably, its concentration is visibly higher for a 4-km/s flow.

The quantitative comparison of the distribution of the total mass flux along the rocket body for different freestream velocities is given in Fig. 18. The maximum mass flux observed on the conical part of the body increases about three times for a change in velocity from 2 to 3 km/s. As the velocity is increased to 4 km/s, the maximum mass flux increases an additional 50%.

Freestream-Plume Interaction at 80 km

In earlier sections the jet-atmosphere interactions were studied for an altitude of 100 km. To examine the influence of the altitude (i.e., ambient pressure) on the flow, the case of 80 km was also considered. The results are presented in this section for a 3250-N thruster at 2 km/s and zero angle of attack. The plume H_2O number density contours are shown in Fig. 19 (top). The impact of the freestream is clearly seen in this case. There is a significant compression layer produced at the windward side of the plume, with the lee side being almost unchanged as compared to Fig. 10.

The freestream N_2 number density field is presented in Fig. 19 (bottom). The shock front formed as a result of the freestream-plume interaction shifts significantly downstream as compared to the higher-altitude case (Fig. 11). The ratio of the number density to the freestream value is larger inside the shock than that for 100 km, which indicates a higher excitation of internal degrees of freedom. An important observation from the study is that the number of chemical reactions between the freestream and plume species is orders of magnitude smaller at 80 km than for 100 km. The number of chemical reactions is larger at 100 km because these reactions are mostly caused by the interaction of freestream particles moving at 2 km/s with plume molecules that move at about 3 km/s. At 100 km many freestream particles penetrate through the shock and reach the plume with no collisions, still having therefore about 2 km/s. At 80 km the freestream gas is much denser, which therefore minimizes the chances of a collision of plume molecules with high-speed particles coming directly from the freestream.

Significant changes in the flow structure for 80 km compared to 100 km are responsible for a qualitative change in the mass flux to the surface for the plume and freestream species. The mass-flux distributions at 80 km for the freestream N_2, plume H_2, and total are given in Fig. 20. The main conclusion from the figures is that the total mass flux for this case is mostly caused by the freestream species N_2 and O_2. Molecular hydrogen gives the biggest contribution from the plume species and is approximately one order of magnitude smaller than the freestream species. A comparison of the total mass flux with the case of no plume shows that the effect of the plume is negligible along the first 1.2 m of the body. The reduction of the mass flux on the cylindrical portion as a result of the presence of the plume is less at 80 km compared to 100 km (see Fig. 14).

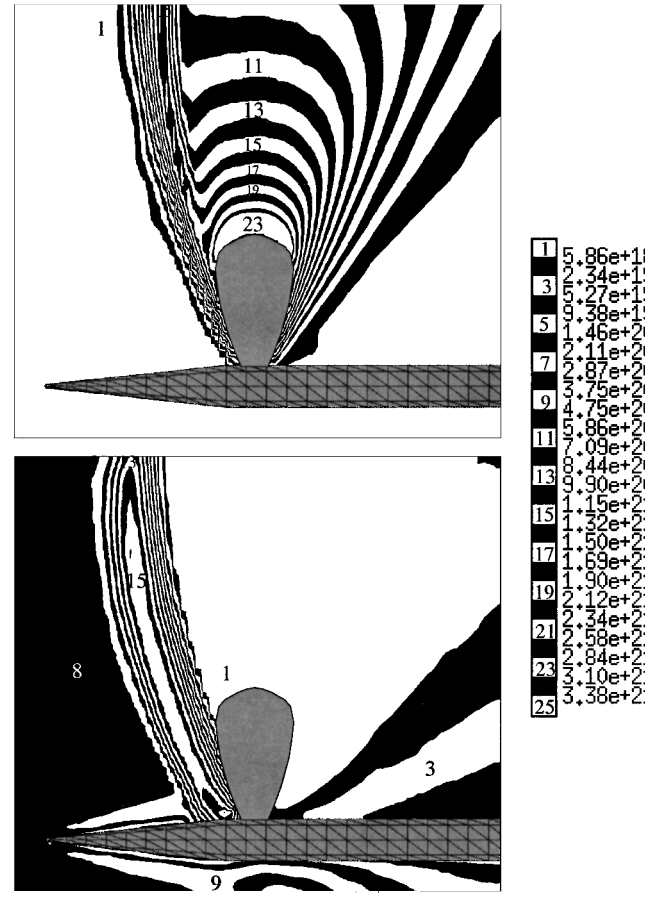

Fig. 19 Plume H_2O (top) and freestream N_2 (bottom) number density contours at 80 km. The area shown is 4.7 × 4.2 m.

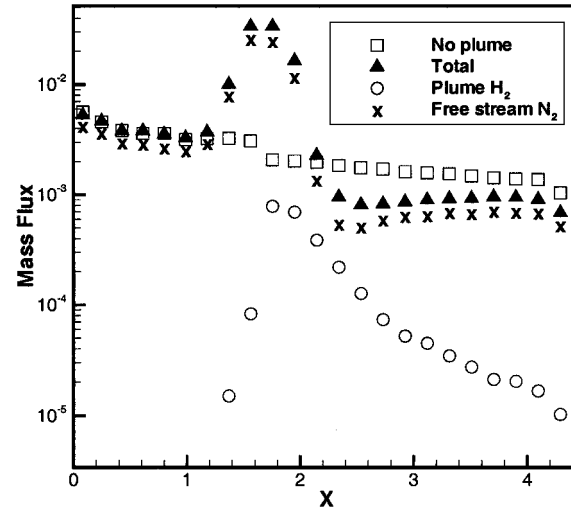

Fig. 20 Total and different species mass flux (kg/m^{2}s) along a rocket at 80 km.

Influence of an Increase in Plume Thrust

Two values of plume thrust are considered in this work, 3250 and 6500 N. The results are given here for the freestream velocity of 2 km/s and a zero angle of attack. Generally, the flowfield structure for a 6500-N thruster is similar to that for the 3250-N case. The freestream N_2 number density field for a 6500-N thruster is shown in Fig. 21. Comparing this result to that for a 3250-N thruster (Fig. 11), one can see that although the flow structure is similar there are some differences. A higher thrust causes a more pronounced shock wave. The freestream molecules are more efficiently moved from the body by the denser plume, and there is a smaller impact of the freestream-plume interaction upstream toward the rocket nose.

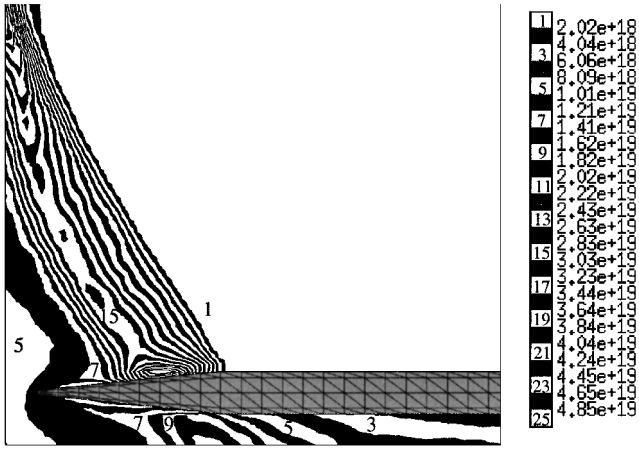

Fig. 21 Freestream N_2 number density contours for $F = 6500$ N at 100 km. The area shown is 4.7 × 4.2 m.

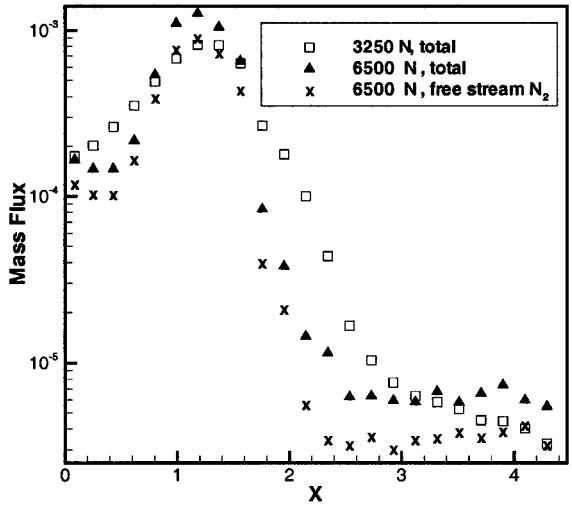

Fig. 22 Comparison of the mass flux (kg/m^{2}s) for different plume thrust values.

This is more clearly seen in the distribution of the mass flux along the body for two different thrust values (Fig. 22). The impact of the plume on the mass flux in the vicinity of the nose is smaller for a 6500-N thruster, which explain a local maximum at the nose tip (same as with no plume). From the nozzle exit to about 1 m downstream, the mass flux is larger for the lower-thrust case as a result of a weaker shadowing effect of the jet. On the last portion of the cylinder, the mass flux is slightly larger for the 6500-N case. This corresponds to a larger number density of the freestream species (compare Figs. 11 and 21). There is some contribution of plume species (mostly hydrogen, up to 20%) for the 6500-N case on the cylindrical part, too.

Influence of the Angle of Attack

To analyze the effect of the angle of attack on the surface mass flux, the computations were performed for four different cases: a) $\alpha = 0$ deg, $\beta = 0$ deg; b) $\alpha = -20$ deg, $\beta = 0$ deg; c) $\alpha = 20$ deg, $\beta = 0$ deg; and d) $\alpha = 0$ deg, $\beta = 20$ deg. Here, α is the angle between the X axis and the projection of the freestream velocity vector on the XY plane, and β is the angle between the X axis and the projection of the freestream velocity vector on the XZ plane. A positive value of α means that the freestream comes from below (see Fig. 6).

The impact of the angle of attack was studied for a 3250-N thruster at an altitude of 100 km and freestream velocity of 2 km/s. The total number density fields for all of the cases are presented in Fig. 23. The amount of plume molecules is negligible in the XZ plane ($Y = 0$), and the fields were therefore normalized by the freestream value. Only half of the computational domain is shown for the three cases

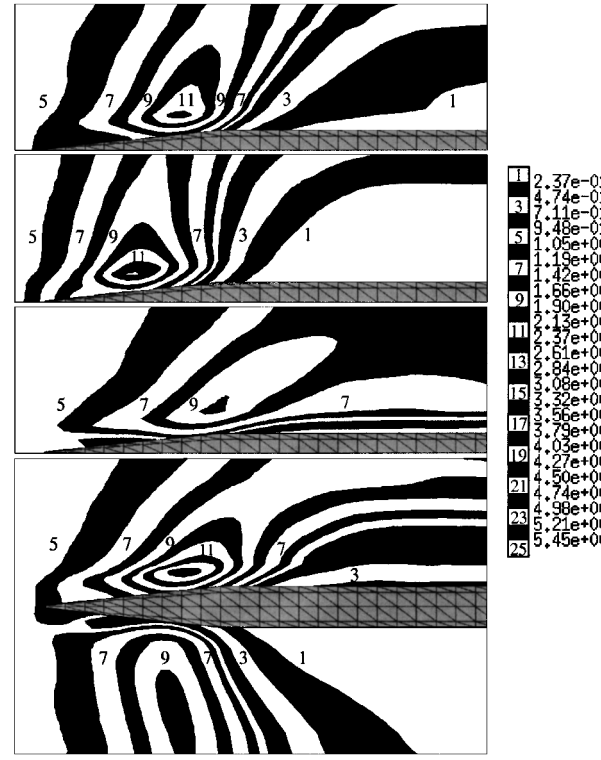

Fig. 23 Normalized number density contours about a rocket for different angles of attack. XZ plane ($Y = 0$). From the top to the bottom: a) $\alpha = 0$, $\beta = 0$; b) $\alpha = -20$ deg, $\beta = 0$ deg; c) $\alpha = 20$ deg, $\beta = 0$ deg; and d) $\alpha = 0$ deg, $\beta = 20$ deg. The area shown is 4.7 × 1.5 and 4.7 × 3 m.

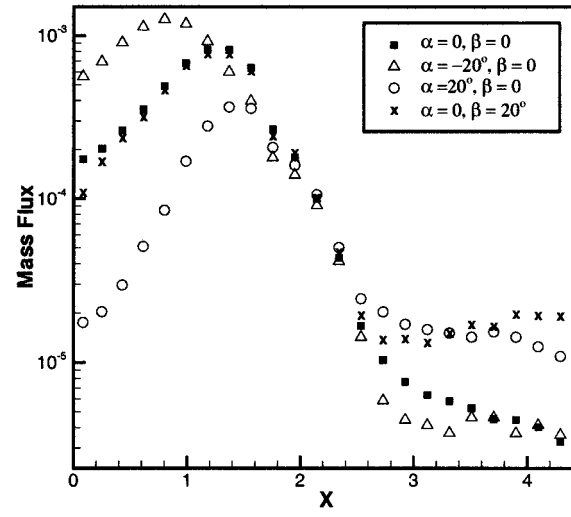

Fig. 24 Total mass flux (kg/m^{2}s) along a rocket for different angles of attack.

because the flow is symmetric with respect to the XY plane. Generally, the influence of the plume is smallest for a positive α. The flow comes from below in this case and therefore minimizes the impact of the plume near the surface. For a negative α the number density near the cylindrical part is a minimum because this area is greatly shadowed by the plume. A maximum number density (about two times larger than in the freestream) is observed at the windward side for $\beta = 20$ deg. The influence of the plume for the lee side is also clearly seen for this case.

The surface distributions of the total mass flux are shown in Fig. 24 for different angles of attack. For the highly rarefied conditions under consideration, the distributions are mostly influenced by the effects of plume and body shadowing and the reflection of freestream molecules from the plume core flow. On the conical portion of the body, the mass flux is a minimum when the freestream comes from below (again, the mass flux is calculated at the upper portion of the

body) and maximum for the opposite case of α. In the vicinity of the nozzle exit, the mass flux strongly decreases, weakly depending on the angle of attack. It increases slightly towards the body end for $\beta = 0$ deg. For the other three cases the mass flux decreases gradually, being a maximum at positive α, when the plume shadowing is smallest. The general conclusion is that if the radiance sensor is located within 0.5 m downstream from the nozzle (X values from 2.1 to 2.6 m), the corresponding mass flux will change within a factor of two for small changes in the angle of attack.

Conclusions

The interaction of a continuum jet, located on the side of a small rocket, with a rarefied atmosphere of 80 and 100 km is studied using the DSMC method. The goal of the modeling was to examine the effect of possible contamination of an onboard radiance sensor located on the cylindrical part of the rocket. The results presented for the flowfields and surface mass flux enable one to evaluate this effect for different freestream and plume conditions.

The numerical procedure consisted of two major steps: calculation of the essentially axisymmetric plume core flow using a two-dimensional code and a successive application of a three-dimensional code to model the plume-freestream interaction. The latter also included the interaction of the freestream and the rocket body. In the first step a computation of the plume near field with GASP solving the Navier–Stokes equations and two-dimensional SMILE using the DSMC approach was performed. The reliable grid- and particle-independent solution of the first stage was used to generate a starting surface for the second step, which used the three-dimensional SMILE code. Chemical reactions between plume and freestream species were included in this step.

The calculations were performed for different thrust values, altitudes, angles of attack, and rocket velocities. The following conclusions about the complex flow structure can be drawn based on the results of the calculations.

At 100 km the contribution of plume species to the mass flux on the surface is mostly caused by molecular hydrogen. This contribution amounts to almost 100% at the first 50 cm of the body downstream of the nozzle exit. The contribution of heavier plume species is negligibly small. For the lower altitude of 80 km, the mass flux is mostly determined by the freestream species N_2 and O_2.

The impact of the freestream on the plume core flow is small at 100 km, but at 80 km it becomes very important. On the contrary, the number of chemical reactions between the freestream and plume species is much bigger at 100 km than at 80 km as a result of the effect of a direct penetration of high-energy freestream molecules through the shock layer to the plume.

Change in the rocket velocity from 2 to 4 km/s increases the number of chemical reactions between the freestream and plume species about five times, producing such species as Cl and OH. Such a change also generates a three to five times rise in the mass flux on the cylinder part of the rocket.

Increase in the plume density reduces the upstream influence of the plume and causes a reduction up to 10 times in the mass flux on the rocket surface along the first 0.5 m downstream from the nozzle exit. The mass flux becomes comparable to the lower-thrust case further downstream.

A change in the angle of attack within 20 deg in either direction does not significantly impact the mass flux on a sensor located within 0.5 m downstream of the nozzle exit. The angle of attack significantly affects the flowfield farther downstream, though, as well as on the conical part of the rocket.

Acknowledgments

The research at Pennsylvania State University and George Washington University was supported by the Space and Naval Warfare Systems Center, San Diego, Califonia, Grant DUNS:04-399-0498 and Army Research Office Grant DAAG55-98-1-009. These programs are supported by the Science and Technology Directorate of the Ballistic Missile Defense Organization, which is conducting programs to characterize and measure the optical radiation from rocket plumes with high spatial resolution. We would like to specifically thank Clifton Phillips for his assistance in securing computer time on the U.S. Department of Defense High-Performance Super Computers, without which these calculations would not be possible, and Jay Levine for his valuable comments and suggestions through the work.

References

[1]Tartabini, P. V., Wilmoth, R. G., and Rault, D. F. G., "Direct Simulation Monte Carlo Calculation of a Jet Interaction Experiment," *Journal of Spacecraft and Rockets*, Vol. 32, No. 1, 1995, pp. 75–83.

[2]Glass, C. E., and LeBeau, G. J., "Numerical Study of a Continuum Sonic Jet Interacting with a Rarefied Flow," AIAA Paper 97-2536, June 1997.

[3]Kanipe, D. P., "Plume/Flowfield Jet Interaction Effects on the Space Shuttle Orbiter During Entry," AIAA Paper 82-1319, Aug. 1982.

[4]Allegre, J., and Raffin, M., "Experimental Study on Control-Jet/Corner-Flow Interaction," Societe d'Etudes et de Services pour Souffleries et Installations Aerothermodynamiques, SESSIA 1759/92.1133, Levallois-Perret, France, Nov. 1992.

[5]Gilmore, M. R., and Warburton, K., "Axisymmetric Hypersonic Jet Interaction: a Combined Experimental and Computational Study II," AIAA Paper 95-0414, Jan. 1995.

[6]Hudson, D., Trolier, J., and Harris, T., "Hot Jet and Mach Number Effects on Jet Interactions Upstream Separation," *1998 AIAA Missile Sciences Conference Proceedings*, Vol. 1, AIAA, Reston, VA, 1998, pp. 654–665.

[7]Glass, C. E., "A Parametric Study of Jet Interactions with Rarefied Flows," *Proceedings of the 21st International Symposium on Rarefied Gas Dynamics*, edited by R. Brun, R. Campargue, R. Gatignol, and J.-C. Lengrand, Vol. 1, Cepadues Editions, Toulouse, France, 1998, pp. 615–622.

[8]Ebrahimi, H. B., "Numerical Simulation of Transient Jet-Interaction Phenomenology in a Supersonic Free Stream," *Journal of Spacecraft and Rockets*, Vol. 37, No. 6, 2000, pp. 713–719.

[9]Nickerson, G. R., Coates, D. E., Dang, A. L., Dunn, S. S., Berker, D. R., Hermsen, R. L., and Lamberty, J. T., "The Solid Propellant Motor Performance Prediction Computer Program (SPP)," U.S. Air Force Astronautics Lab., TR-87-078, Edwards AFB, CA, Dec. 1987.

[10]Moss, J. N., Bird, G. A., and Dogra, V. K., "Nonequilibrium Thermal Radiation for an Aeroassist Flight Experiment Vehicle," AIAA Paper 88-0081, Jan. 1988.

[11]Bird, G. A., "Simulation of Multi-Dimensional and Chemically Reacting Flows," *Rarefied Gas Dynamics,* Vol. 1, edited by R. Campargue, Commissariat a Lenergie Atomique, Paris, 1979, pp. 365–388.

[12]Ivanov, M. S, Markelov, G. N., and Gimelshein, S. F., "Statistical Simulation of Reactive Rarefied Flows: Numerical Approach and Applications," AIAA Paper 98-2669, June 1998.

[13]"GASP Version 3, The General Aerodynamic Simulation Program, Computational Flow Analysis Software for the Scientist and Engineer, User's Manual," Aerosoft Co., Blacksburg, VA, May 1996.

[14]Gimelshein, S. F., Ivanov, M. S., and Rogasinsky, S. V., "Investigation of Shock Wave Structure by Majorant Cell and Free Cell Schemes of DSMC," *Proceedings of the XVII International Symposiun on Rarefied Gas Dynamics*, edited by A. E. Beylich, VCH, Weinheim, Germany, 1991, pp. 718–726.

[15]Bird, G. A., *Molecular Gas Dynamics and the Direct Simulation of Gas Flows*, Clarendon, Oxford, 1994, pp. 2–4.

[16]Bird, G. A., "Monte-Carlo Simulation in an Engineering Context," *Rarefied Gas Dynamics*, edited by S. Fisher, Vol. 74, Progress in Astronautics and Aeronautics, AIAA, New York, 1981, pp. 239–255.

[17]Borgnakke, C., and Larsen, P. S., "Statistical Collision Model for Monte Carlo Simulation of Polyatomic Gas Mixture," *Journal of Computational Physics*, Vol. 18, No. 4, 1975, pp. 405–420.

[18]Gimelshein, S. F., Levin, D. A., and Collins, R. J., "Modeling of Spacecraft Glow Radiation in Flows About a Reentry Vehicle at High Altitudes," *Journal of Thermophysics and Heat Transfer*, Vol. 14, No. 4, 2000, pp. 471–479.

I. D. Boyd
Associate Editor